Organic & Biomolecular Chemistry

ROYAL SOCIETY OF CHEMISTRY

PAPER

View Article Online
View Journal | View Issue

Cite this: *Org. Biomol. Chem.*, 2021, **19**, 1589

Unravelling the potency of triazole analogues for inhibiting α-synuclein fibrillogenesis and *in vitro* disaggregation†

Mudasir Maqbool,[a] Joshna Gadhavi,[b] Anju Singh,[a] Pravin Hivare,[b] Sharad Gupta*[b] and Nasimul Hoda *[a]

Received 8th November 2020,
Accepted 22nd January 2021

DOI: 10.1039/d0ob02226h

rsc.li/obc

A series of triazole-based compounds was synthesized using a click chemistry approach and evaluated for the inhibition of α-synuclein (α-syn) fibrillogenesis and its disaggregation. Compounds **Tr3**, **Tr7**, **Tr12**, **Tr15**, and **Tr16** exhibited good effect in inhibiting α-syn fibrillogenesis confirmed by Thioflavin-T assay and fluorescence microscopy and α-syn disaggregation confirmed by fluorescence microscopy. Molecular docking was used to understand the plausible mechanism of the test compounds for inhibiting the α-syn fibrillogenesis and to verify the *in vitro* results. Compounds **Tr3**, **Tr7**, **Tr12**, **Tr15** and **Tr16** showed good binding interactions with the essential amino acid residues of α-syn. The compounds which were found to be good inhibitors or disaggregators had no toxic effects on the SH-SY5Y cell line. These compounds have the potential to be developed as therapeutic interventions against synucleinopathies including Parkinson's disease and Lewy body dementia.

Introduction

Parkinson's disease (PD) is a hypokinetic movement disorder and the second most common neurodegenerative disease (ND) after Alzheimer's.[1,2] Globally, the burden of PD has doubled over the past 26 years, from 2.5 million patients in 1990 to 6.1 million patients in 2016.[3] The disease mostly manifests after the age of 65 years; however in approximately 4% of the PD patients, symptoms appear before the age of 50 years.[4] Histopathologically, PD is stated to occur due to abnormal formation and accumulation of fibrillar cytoplasmic protein deposits which mainly consist of α-syn. Besides PD, elevated levels of α-syn along with amyloid protein tau have also been reported in Alzheimer's disease (AD) and Creutzfeldt–Jakob's disease (CJD), suggesting the ambiguous involvement of α-syn in other NDs.[5,6] Lewy bodies and Lewy neurites, the known pathological hallmarks of PD, are predominantly found in the substantia nigra pars compacta and locus ceruleus parts of the brain, while some traces have been found in subcortical and cortical regions. These Lewy bodies affect the dopaminergic neuronal projections from the substantia nigra to the striatum, thereby disturbing the ability to initiate, carry out and control voluntary movements.[7] The persistence of Lewy bodies also alters the acetylcholine content in the brain, thus disrupting the thinking and learning ability of a person. Bradykinesia, rigidity, and motor dysfunction include the early indications of PD; however, cognitive dysfunction has been observed during the later stages of the disease.[8]

The complete physiological effects of α-syn are not well understood. However, α-syn is highly expressed in nuclear synapses and may be involved in neuronal plasticity and protection from apoptosis and oxidative damage.[9] Structurally, α-syn is a 140 amino acid long protein with three distinguished regions: (1) 1–60, containing 11 amino acids having 4 repeats, (2) 61–95, which is hydrophobic and known as the non-amyloid beta component (NAC), and (3) 96–140, a C-terminal region which is acidic.[10] Novel drug candidates that could impede the formation or aggregation of α-syn are regarded as potential therapeutics for PD and related synucleinopathies. ZPD-2, SC-D, 5OHDPAT, Pramipexole, D-519 and D-520 are some of the noteworthy examples of known efficient α-syn inhibitors (Fig. 1).[11–13]

Triazole analogues have been reported to modulate nicotinic acetylcholine receptors and have been proposed to treat central nervous system disorders such as NDs and neuroinflammation.[14] Such compounds have also been reported to inhibit different kinases.[15] 1,2,4-Triazoles have been found to act as antagonists to the human adenosine receptor consequently, and can be used against PD.[16] A series of triazole-

[a]*Drug Design and Synthesis Lab., Department of Chemistry, Jamia Millia Islamia, Jamia Nagar, New Delhi-110025, India. E-mail: nhoda@jmi.ac.in*
[b]*Biological Engineering, Indian Institute of Technology Gandhinagar, Palaj, Gandhinagar, Gujarat, India. E-mail: sharad@iitgn.ac.in*

†Electronic supplementary information (ESI) available. See DOI: 10.1039/d0ob02226h

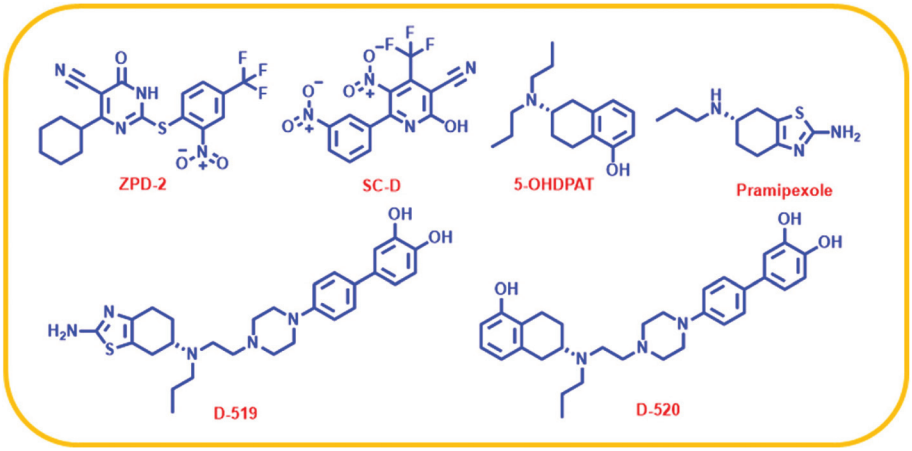

Fig. 1 Structure of some identified potential α-syn inhibitors.[11–13]

based compounds was discovered with a significant anti-aggregation effect on α-syn in the SH-SY5Y cellular model of synucleinopathy.[17] Such compounds have been used for the treatment of AD as they attenuated the production of $A\beta_{42}$.[18] Triazole-based compounds have been reported to inhibit GSK-3 with IC_{50} values in the range of 0.1–10 μM.[19] In addition to triazole, other scaffolds have also shown promise as potential therapeutics for AD and PD treatment. For example, 1,2-dimethoxy benzene containing compounds have recently been tested to inhibit α-syn, NAC peptide, and tau aggregation up to 100%.[20] Benjamin and co-workers recently reported a series of 1,2,4, oxadiazole compounds with a cytoprotective effect in human neurons against α-syn-mediated toxicity.[21] Kozikowski *et al.* have demonstrated that 3-indolyl-4-indazolylmaleimides not only inhibit GSK-3β and block tau phosphorylation but also reduce α-syn expression in a cellular model of PD.[22] Furthermore, a set of 3 (benzylidine)indolin-2-one derivatives displayed significant *in vitro* inhibition of α-syn, Aβ, and tau fibrils.[23]

Considering the above record of accomplishment of different drug moieties, here we synthesized and evaluated the anti-PD effect of a series of triazole core structure-based compounds (**Tr1**, **Tr3**, and **Tr5–Tr18**). Later, to understand the plausible mechanism of action of the molecules we used *in silico* docking and scoring methods. The rationale for designing triazole analogues for the anti-PD effect is illustrated in Fig. 2.

The target molecules were synthesized using azide–alkyne Huisgen cycloaddition reactions. Later, the target molecules

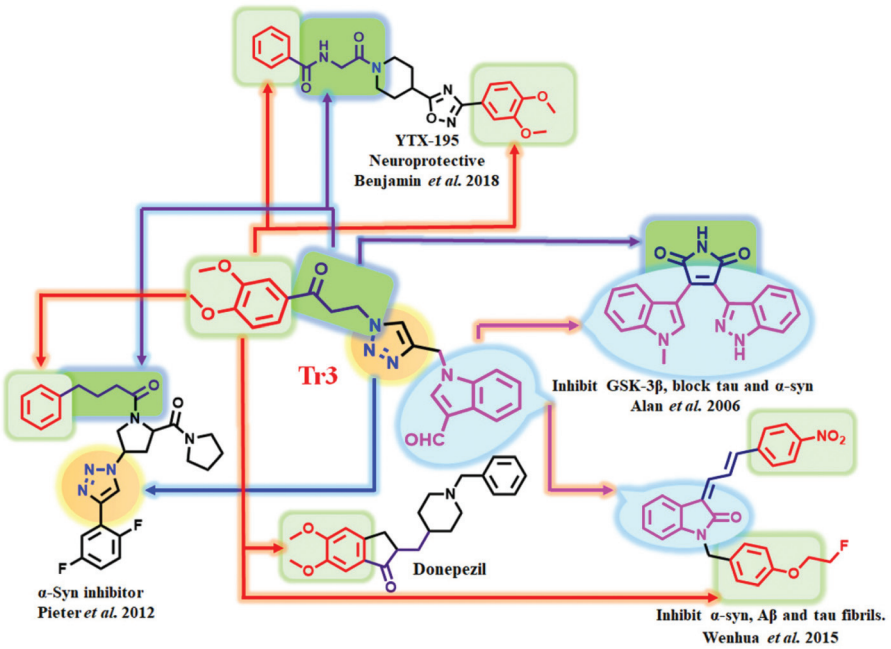

Fig. 2 Motivation for the development of multi-component triazole-based hybrids for α-syn inhibition.

were evaluated for α-syn fibrillogenesis inhibition and disaggregation *in vitro*. The cytotoxic effects of compounds on SH-SY5Y cell lines were tested and flexible docking and redocking were performed to rationalize some of the observations from experimental data.

Results and discussion

Synthesis of triazole analogues

The target compounds were synthesized through multiple steps as illustrated in Schemes S1 and S2† and Table 3. In Scheme S1 (ESI†), differently substituted azides (**3**, **5**, and **7**) were synthesized from compounds **2**, **4** and **6**, respectively. Differently substituted terminal alkynes were synthesized according to the reaction conditions depicted in Scheme S2 (ESI†) and a reported literature method.[24] In Table 3, the synthesized azides (**3**, **5**, and **7**) were coupled with different terminal alkyne containing compounds in the presence of $CuSO_4{\cdot}5H_2O$ and sodium ascorbate ($THF:H_2O$ in a ratio of 1 : 2), under the reflux conditions at 80 °C for 16 h to obtain the target compounds (**Tr1**, **Tr3**, and **Tr5–Tr18**). The structures of these compounds were confirmed from analytical and spectroscopic data (^1H NMR, ^{13}C NMR and mass spectra).

Biological evaluation synthesized compounds

Recombinant α-syn protein purification. α-Syn protein was expressed in *Escherichia Coli* BL21 (DE3) and extracted using the osmotic shock method as previously reported.[25,26] Purification was performed on Diethyl Amino Ethyl (DEAE) Sepharose using ion-exchange chromatography. The eluted fractions containing α-syn protein were identified by 15% SDS-PAGE as shown in Fig. 3A, and after pooling, they were dialyzed against water at 4 °C to ensure complete removal of residual salts which could interfere with the aggregation assays. Western blot was performed using the H3C monoclonal antibody specific for α-syn that gave a single band at ~16 kDa as shown in Fig. 3B.[26]

Aggregation kinetics of α-syn fibrillization in the presence of Tr-series inhibitors. α-Syn aggregation progress can be monitored in real-time using ThT, a benzothiazole based dye which fluoresces very strongly (Ex: 445 nm, Em: 485 nm) when bound to amyloid structures. To assess the inhibitory potential of the Tr-series compounds, α-syn (70 μM) was mixed with compounds dissolved in DMSO in a 1 : 1 molar ratio along with ThT (20 μM), and the evolution of ThT fluorescence was observed in real-time. The final concentration of DMSO was fixed at 10% and as a control, DMSO without an inhibitor was mixed with α-syn. From the nucleation dependent sigmoidal ThT fluorescence curve (Fig. 4), a characteristic of amyloid-like behavior was obtained for the control and α-syn incubated with the test compounds at an equimolar ratio (except **Tr18**, Fig. 4l). Nevertheless, significant differences were detected for various kinetics parameters (Fig. 4 and Table 1), revealing the inhibitory effects of several test compounds.

Although the absolute quantification of amyloid formation from ThT fluorescence values is not possible, final plateau fluorescence (F_{final}) can give a relative estimation of β-sheet rich structures that allows a direct comparison of the inhibitory potential.[27,28] A lower value of F_{final} would imply stronger inhibition. As shown in Fig. 4b, e, i, j, k and 5, **Tr3**, **Tr7**, **Tr12**, **Tr15** and **Tr16** significantly lowered the F_{final} ($p < 0.001$) with values declining by more than 50% when compared to the control (α-syn without an inhibitor). For **Tr5**, **Tr9** and **Tr11** a drop in F_{final} was significant ($p < 0.01$) and the reduction in values was less than 30%. **Tr1**, **Tr6** and **Tr10** did not show any significant inhibition, while **Tr18** displayed a peculiar behavior with fluorescence values starting at a high level and declining steadily over time. Interference from self-aggregation was ruled out by separate long-term (>2 weeks) incubation of the test compounds along with ThT without α-syn which led to no significant change in ThT fluorescence (data not shown).

From the ThT fluorescence curve, we further calculated t_{lag}, $t_{1/2}$ (time required to arrive halfway of the elongation phase) and k_{app} (apparent elongation rate constant for fibrillar growth) based on the method reported by Gade Malmos *et al.*[29] As shown in Table 1, there was no significant elongation of the lag phase observed for any of the compounds tested except **Tr10**, which implied that the **Tr** series compounds did not interfere with the early nucleation event. However, for **Tr10**, both t_{lag} and $t_{1/2}$ were halved which suggested its role as a facilitator of fibrillation rather than an inhibitor. In addition, for **Tr6** we observed some lengthening of $t_{1/2}$ but other compounds showed no significant changes. As far as top inhibitors are concerned, **Tr3**, **Tr7** and **Tr15** gave a higher k_{app} than the control hinting at slowing down of the fibrillization process. Only **Tr12** exhibited acceleration of fibrillization but when taken together with non-significant changes in t_{lag} and $t_{1/2}$ along with low F_{final}, a premature termination of fibrillization appears to be the most likely explanation.

As is evident from the above analysis, even though some compounds performed very well (*e.g.* **Tr3** or **Tr16**) full inhibition was not achieved for the equimolar ratio of an inhibitor to protein, a characteristic of thermodynamic inhibitors of aggregation.[28] An inhibitor can also bind to non-amyloidogenic regions thereby reducing the inhibitory potential for the initial phase of aggregation. In later phases though, the stoichiometric ratio favors the inhibitor that prematurely halts the fibrillar growth that is reflected in the lower F_{final} than that of the positive control. Our attempts to try out a significantly higher ratio of an inhibitor to protein by reducing the α-syn concentration or increasing it did not go very far as a lower concentration of α-syn led to extension of the aggregation time span and low solubility of inhibitory compounds, respectively.

Microscopic analysis of α-syn fibrillogenesis and disaggregation. After reaching the plateau phase in the ThT aggregation assay as shown in Fig. 6, fluorescence microscopy images were recorded to confirm the inhibitory potential of compounds. As the samples were withdrawn directly from the ThT aggregation assay, ThT was already intercalated within fibrillar aggregates and was fluorescently active which can be seen through an

Table 3 Synthesis of desired compounds using azide–alkyne Huisgen's cycloaddition method

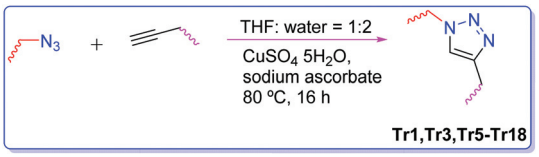

Azides	Terminal alkyne groups	Target compounds	Yield obtained
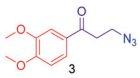	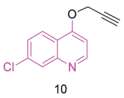	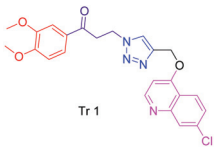	76%
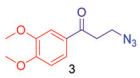		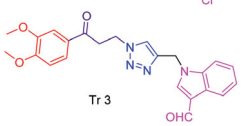	80%
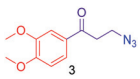		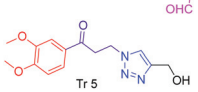	70%
	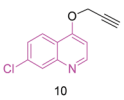	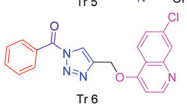	66%
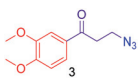	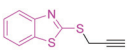	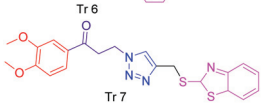	61%
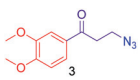	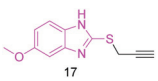	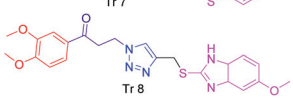	66%
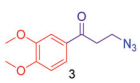	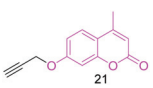	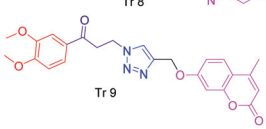	72%
	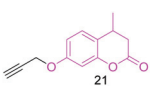	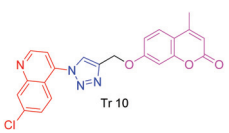	68%
		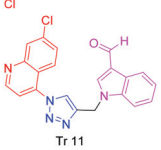	69%
	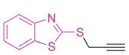	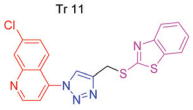	70%
	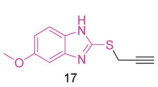	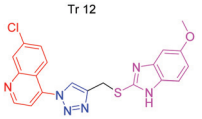	61%
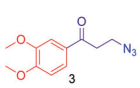	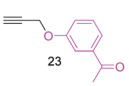	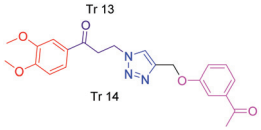	74%
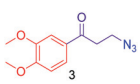	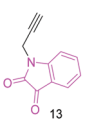	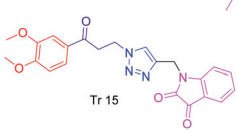	67%

Table 3 *(Contd.)*

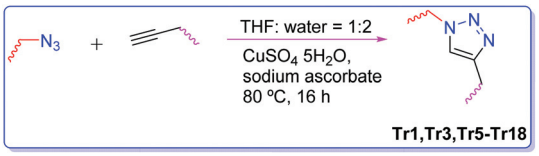

Azides	Terminal alkyne groups	Target compounds	Yield obtained
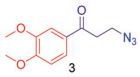	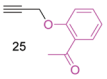	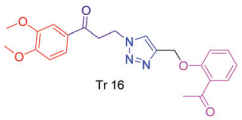	78%
	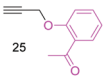	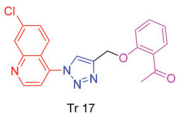	75%
	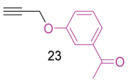		66%

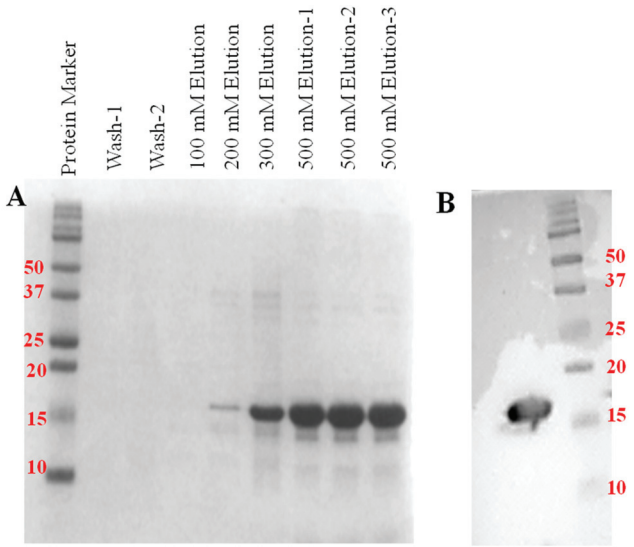

Fig. 3 Characterization of purified α-syn by SDS-PAGE and western blot. (A) Analysis of purified α-syn fractions on 15% SDS-PAGE eluted with different NaCl concentrations. (B) Western blot analysis of purified α-syn, primary antibody: H3C and secondary: anti-mouse HRP conjugated antibody.

FITC filter under a fluorescence microscope. Brightly illuminated fibrillar aggregates in high abundance were present in the α-syn only sample (control) as shown in Fig. 6a. However, α-syn samples treated with test compounds **Tr3**, **Tr7**, **Tr11**, **Tr12**, **Tr15** and **Tr16** had only sparsely populated brightly illuminated punctuates as shown in Fig. 6. This was in line with the observations from *in vitro* ThT aggregation assay (Fig. 4) where all of the above compounds except **Tr11** exhibited at least 50% inhibition with $p < 0.001$. **Tr1**, **Tr5** and **Tr6** showed fibrillary aggregates qualitatively similar to the control as shown in Fig. 6b, d and f. Intriguingly **Tr9** showed more diffused aggregates decorated with some bright dots, which made the classification ambiguous.

Molecules which have the capacity to dissolve preformed aggregates have a much higher potential as a therapeutic lead than those which only inhibit the conversion of monomers to fibrillar aggregates. Hence, we further evaluated all the test compounds for disaggregation activity. Accordingly, α-syn fibrillar aggregates pre-formed without ThT were incubated with the Tr-series compounds (molar ratio: 1 : 1) at 37 °C for 4–5 days. Before imaging, ThT was mixed with the samples and images were captured under a microscope through the FITC filter. Brightly illuminated fibrillar aggregates were observed in the control α-syn sample as shown in Fig. 7A. **Tr5** and **Tr6** had virtually no impact on the aggregates (Fig. 7D and E); however **Tr1** and **Tr9** appear to partially dissolve α-syn aggregates as is evident from a qualitative comparison of Fig. 7B and G with 7A. Unsurprisingly **Tr3**, **Tr7**, **Tr11**, **Tr12**, **Tr15** and **Tr16** which efficiently inhibited the conversion of monomeric α-syn into fibrillar aggregates (Fig. 5 and 6) were also very effective in disaggregating the preformed aggregates. For these samples, generally, the entire area of the microscopic slide was blank and it was difficult to find regions with bright spots. We could only find a very few regions with some brightness and one such representative image for each sample has been provided in Fig. 7C, F and H–K. Overall, these results from the disaggregation test corroborate the findings from ThT aggregation inhibition assay and microscopic confirmation indicating that the above listed compounds have therapeutic potential against α-syn fibrillogenesis.

***In silico* studies of triazole-based α-syn inhibitors.** To understand the plausible mechanism of triazole-based molecules for inhibiting α-syn fibrillogenesis *in vitro*, we relied upon molecular docking. The binding energy values and docking inter-

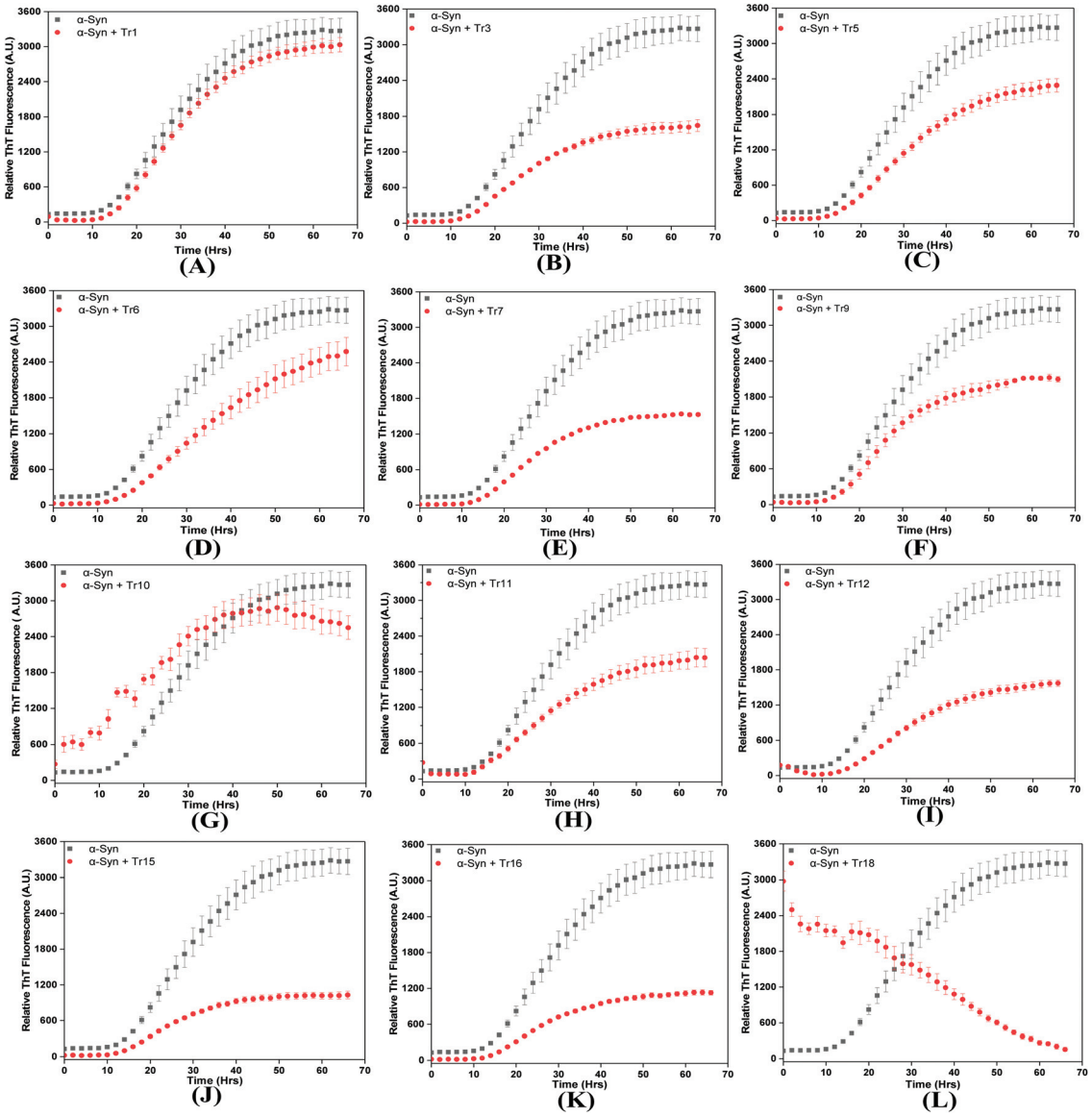

Fig. 4 Aggregation kinetics of α-syn fibril formation with (Tr series) and without compounds in the presence of ThT. Thioflavin-T fluorescence assay of the aggregation of α-syn in the presence of (A) **Tr1**, (B) **Tr3**, (C) **Tr5**, (D) **Tr6**, (E) **Tr7**, (F) **Tr9**, (G) **Tr10**, (H) **Tr11**, (I) **Tr12**, (J) **Tr15**, (K) **Tr16 and** (L) **Tr18**. Here, black dots indicate ThT fluorescence values for α-syn only and red dots indicate α-syn incubated with the Tr series compounds. Here, data represent ± SEM of three independent replicates.

Table 1 Fitted parameters from the ThT fluorescence curve such as $t_{1/2}$, t_{lag}, and k_{app} for α-syn incubated with or without the inhibitors

Aggregation series	$t_{1/2}$ (h)	t_{lag} (h)	k_{app} ($\times 10^{-3}$ h^{-1})
α-Syn	27.4 ± 0.9	13.8 ± 0.3	108.5 ± 5.9
α-Syn + **Tr1**	28.5 ± 0.6	14.9 ± 0.5	111.5 ± 3.8
α-Syn + **Tr3**	26.2 ± 1.7	14.1 ± 0.6	139.0 ± 3.7
α-Syn + **Tr5**	30.1 ± 1.3	14.5 ± 0.6	109.9 ± 3.4
α-Syn + **Tr6**	33.7 ± 1.2	14.8 ± 0.4	95.3 ± 1.8
α-Syn + **Tr7**	26.1 ± 0.2	14.0 ± 0.1	120.0 ± 0.1
α-Syn + **Tr9**	25.6 ± 1.0	15.5 ± 0.6	111.2 ± 6.6
α-Syn + **Tr10**	13.0 ± 1.8	5.8 ± 1.1	106.1 ± 13.8
α-Syn + **Tr11**	27.4 ± 0.7	12.7 ± 0.4	73.2 ± 1.1
α-Syn + **Tr12**	29.5 ± 0.8	15.1 ± 0.7	70.9 ± 4.3
α-Syn + **Tr15**	23.9 ± 0.2	13.3 ± 0.4	134.7 ± 22.0
α-Syn + **Tr16**	25.6 ± 0.2	13.5 ± 0.2	107.5 ± 3.5

actions of ligands with α-syn further help us rationalize the *in vitro* results. For flexible docking and redocking, AutoDock Vina version 1.5.6 was used. The simulation boxes during docking were developed to conceal the interacting residues of the protein and the ligand.[30] The docking results provided the approximate binding affinity ($-\Delta G$ in kcal mol^{-1}) between the ligand and α-syn (PDB ID 1XQ8) as mentioned in Table 2. The aromatic systems joined *via* a combination of flexible and rigid linkers are expected to favor non-covalent interactions with the binding site residues of α-syn *e.g.* π–π stacking interactions and hydrogen bonding. Apparently, alkyl or aryl groups with varying degrees of hydrophobicity and electronic properties determined the binding affinity of the ligands to α-syn. The

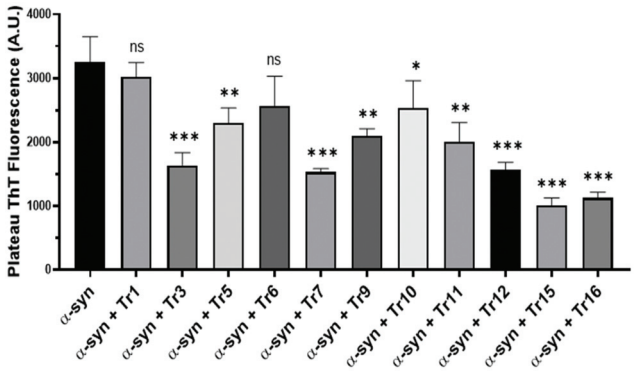

Fig. 5 Plateau ThT fluorescence for α-syn fibrillization reaction in the presence of Tr-series inhibitors. Here, data represent the average of fluorescence values from four different wells after fibrillization *i.e.* the plateau phase. *** = $p < 0.001$, ** = $p < 0.01$ and * = $p < 0.05$, ns = non-significant when compared against α-syn fibrillization in the absence of the inhibitor.

binding free energies of the five best compounds **Tr3**, **Tr7**, **Tr12**, **Tr15** and **Tr16** with α-syn were found to be −6.8, −6.9, −7.0, −7.5 and −7.7 kcal mol^{-1}, respectively which suggested a very strong affinity of ligands towards α-syn. These five compounds displayed a higher degree of *in vitro* inhibition of α-syn fibrillogenesis as shown in Fig. 6 and ostensibly, docking results validated our observations from ThT fluorescence-based aggregation assay.

The NAC region of α-syn, consisting of a tyrosine triad (Tyr125, Tyr133, and Tyr136) plays a key role in fibrillogenesis and binding of presumed inhibitors to this site may prevent the α-syn fibrillogenesis and aggregation.[31–33] The interpretation of the docking results revealed that: indole and dimethoxyphenyl systems of **Tr3** interact with Tyr136 and Tyr125, respectively, *via* π–π stacking (Fig. 8a). In addition, a H bond of bond length 3.0 Å was found between nitrogen of triazole and hydrogen of Gly132. Dimethoxyphenyl and benzothiazole groups of **Tr7** showed π–π stacking with Tyr125 and Tyr136, respectively (Fig. 8b). Likewise, chloroquinoline and benzothiazole of **Tr12** appeared to be involved in π–π interactions with Tyr136 and Tyr125, respectively (Fig. 8c). The veratrole functionality in **Tr15** appeared to interact with Tyr125 (Fig. 8d). A strong H bond of bond length 2.3 Å was also found between nitrogen of triazole and hydrogen of Gly132. In the case of **Tr16**, acetophenone and dimethoxybenzene were observed to interact with Tyr136 and Tyr125 through π–π stacking, respectively. Along with that, a H bond of bond length 2.6 Å was also found between nitrogen of triazole and hydrogen of Gly132 (Fig. 8e). Overall, the interpretations reveal that these triazole-based compounds interact well with the essential residues of α-syn through different non-covalent interactions and could be the basis for their *in vitro* α-syn fibrillogenesis inhibition.

Cytotoxicity studies of the Tr-series compound through MTT assay. We exposed SH-SY5Y neuroblastoma cells to the Tr-series compounds and checked the cellular viability using MTT assay. The SH-SY5Y cells were incubated with the Tr

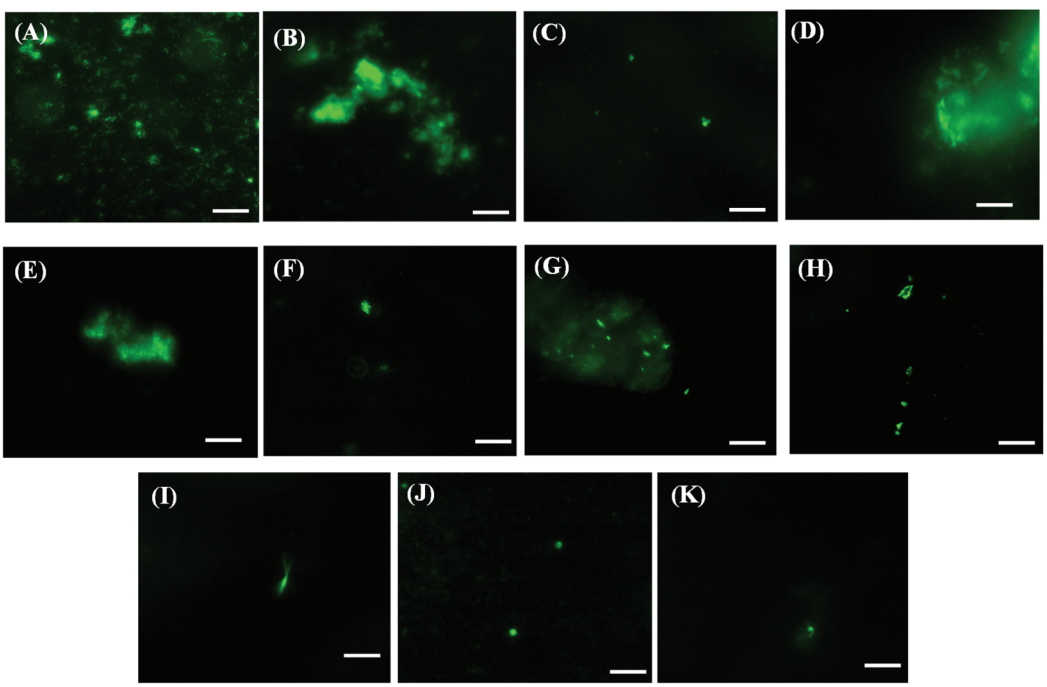

Fig. 6 Post-fibrillization images under a fluorescence microscope showing the impact of the Tr-series compounds on the aggregation of monomeric α-syn. (A) α-Syn aggregation in the absence of any inhibitors. (B–K) α-Syn aggregation in the presence of **Tr1**, **Tr3**, **Tr5**, **Tr6**, **Tr7**, **Tr9**, **Tr11**, **Tr12**, **Tr15** and **Tr16**. Scale bar = 10 μm. Various imaging parameters such as laser power, intensity and zoom level were maintained constant throughout the fluorescence imaging to enable a direct comparison.

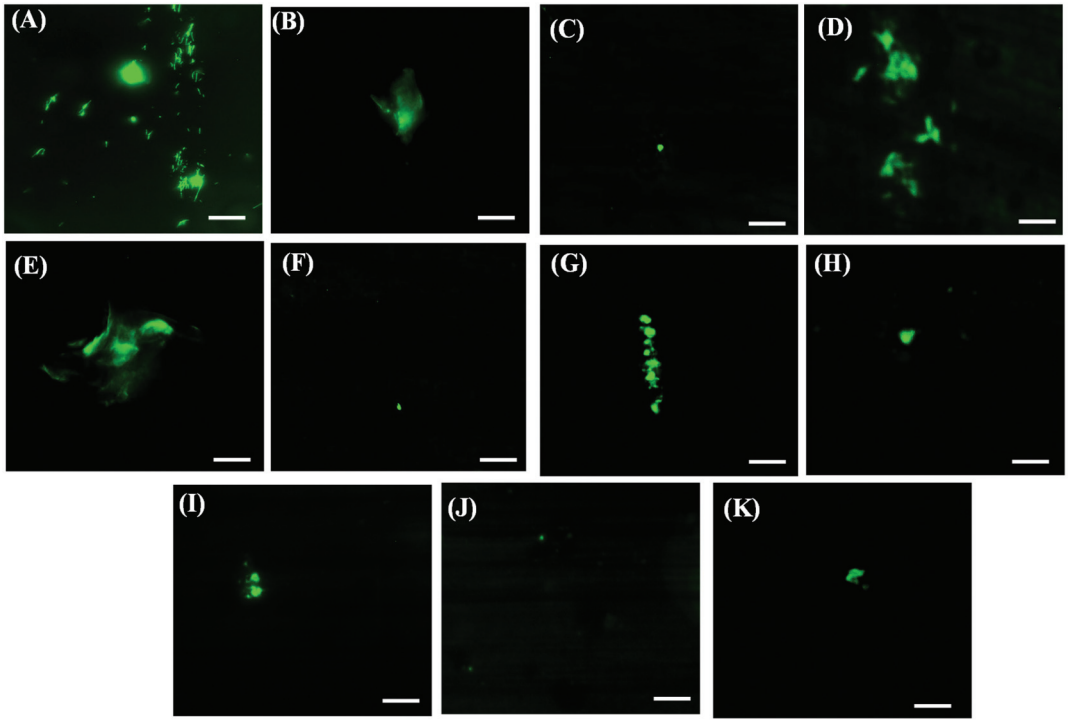

Fig. 7 The effect of the test compounds on α-syn fibrillar aggregates observed under the fluorescence microscope. (A) Aggregated α-syn with no inhibitor. (B–K) Preformed α-syn aggregates incubated for 5 days in the presence of **Tr1**, **Tr3**, **Tr5**, **Tr6**, **Tr7**, **Tr9**, **Tr11**, **Tr12**, **Tr15** and **Tr16**. Here, the scale bar represents 10 μm. Various imaging parameters such as laser power, intensity and zoom level were maintained constant throughout the fluorescence imaging to enable a direct comparison.

Table 2 The calculated free energies of Tr series derivatives from molecular docking using Auto Dock Vina[30]

Compound name	Binding affinity (kcal mol^{-1})
Tr1	−5.6
Tr3	**−6.8**
Tr5	−4.7
Tr6	−5.7
Tr7	**−6.9**
Tr8	−4.9
Tr9	−5.5
Tr10	−6.7
Tr11	−5.6
Tr12	**−7.0**
Tr13	−6.5
Tr14	−5.4
Tr15	**−7.5**
Tr16	**−7.7**
Tr17	−6.2
Tr18	−5.2

α-Syn with PDB ID 1XQ8 was used for calculating the binding affinity of the compounds with the protein. Values in bold represent the most active binding compounds: **Tr3**, **Tr7**, **Tr12**, **Tr15** and **Tr16** with binding affinity values of −6.8, −6.9, −7.0, −7.5 and −7.7 kcal mol^{-1}, respectively.

series compounds at 100 μM concentrations which were 1.5-fold higher than the concentration used for the aggregation kinetics. As shown in Fig. 9, most of the compounds do not show any major loss in cellular viability. **Tr10** appeared to promote cell growth though the difference was nonsignificant compared to the control. **Tr11** was found to be highly cytotoxic ($p < 0.001$) with only less than 20% cell survival. However, **Tr9**, **Tr12**, **Tr15** and **Tr18** also exhibited a significant loss in cellular viability but more than 70% of the cells were viable even after 24 h of incubation. Cells treated with DMSO without any compounds were used as a control. Overall, except **Tr11**, all the compounds were found to be suitable for cell culture-based studies and have the potential to be developed further for *in vivo* applications.

Prediction of blood–brain barrier (BBB) permeability. Crossing the selective semipermeable Blood–Brain Barrier (BBB) is one of the basic criteria to be considered while exploring novel neurotherapeutics.[34] Loreclezole, a modulator of binding at a gamma-aminobutyric acid (GABA) type A receptor is one of the best examples of triazole-based drugs which cross the BBB and work as a sedative and anticonvulsant.[35] Alprazolam, a member of the triazolobenzodiazepine class, which are benzodiazepines fused with a triazole ring, is a short-acting tranquilizer and exhibits dose dependent activity in the central nervous system.[36]

Recently, B. Kaproń *et al.*[37] reported a series of 1,2,4-triazole-3-thione derivatives with robust anticonvulsant activity. They evaluated 9 out of 22 synthesized derivatives using PAMPA (parallel artificial membrane permeability assay)-BBB assay and all of them were found to be BBB penetrant. Shuo-En Tsai *et al.*[38] have also reported a high degree of BBB per-

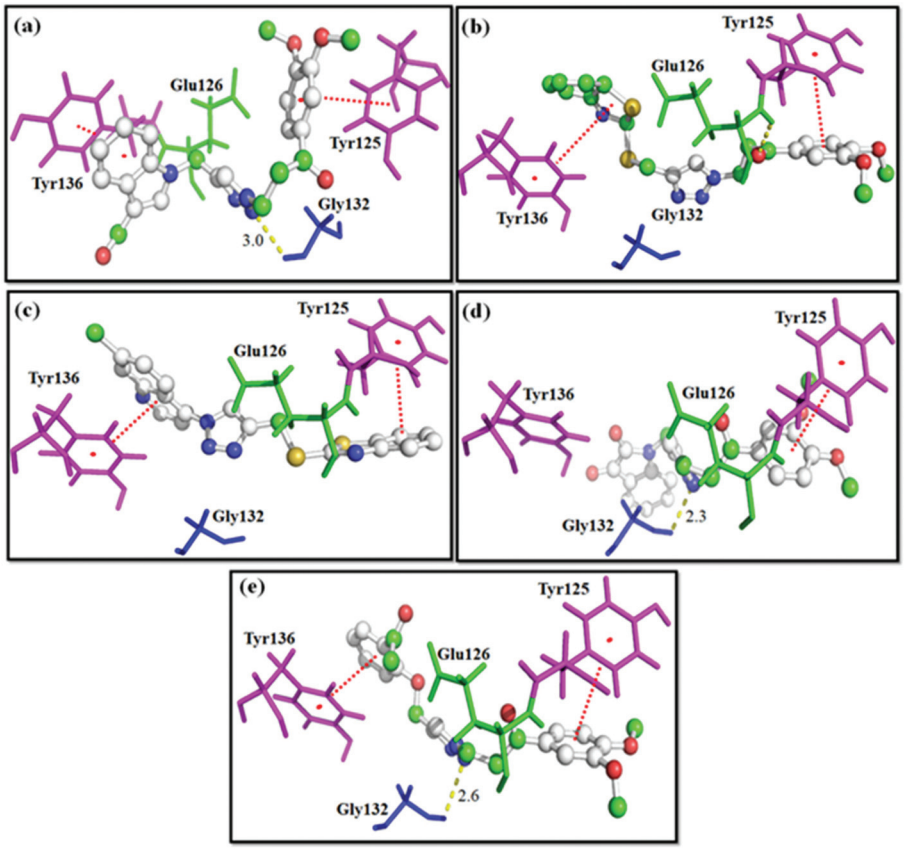

Fig. 8 Molecular interaction of compounds **Tr3**, **Tr7**, **Tr12**, **Tr15** and **Tr16** with α-syn (PDB ID 1XQ8). (a) Interactions of **Tr3** with α-syn. (b) **Tr7** in the binding pocket of α-syn. (c) Interaction between the important residues of α-syn and **Tr12** compound. **Tr15** (d) and **Tr16** (e) interacting with α-syn. Tyr is shown in magenta, Glu in green and Gly in blue. Hydrogen bonding and π–π interactions are shown with yellow and red dotted lines, respectively.

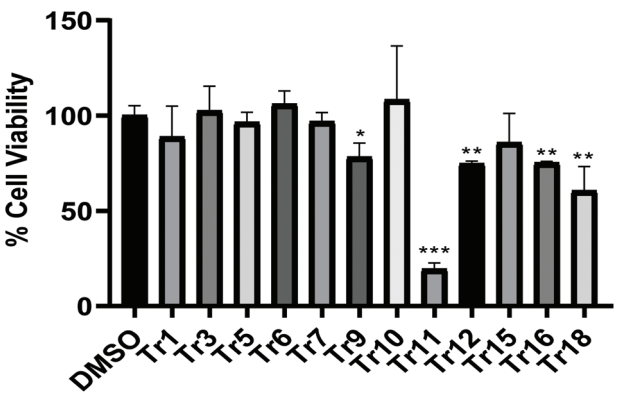

Fig. 9 The % cell viability of SH-SY5Y cells incubated with compounds (**Tr1**, **Tr3**, **Tr5**, **Tr6**, **Tr7**, **Tr8**, **Tr9**, **Tr10**, **Tr11**, **Tr12**, **Tr15**, **Tr16** and **Tr18**) after 24 h of incubation. A 1 mM solution of compounds in DMSO was used for the assay with the final concentration as 100 μM. Cells treated with only DMSO were used as the control. Data represent ± SEM of three independent replicates. *** = $p < 0.001$, ** = $p < 0.01$ and * = $p < 0.05$.

meability for a triazole-based rimonabant analog, a potent and specific CB_1 antagonist, using MDCK-mdr1 permeability assay for BBB penetration.[38] Computational prediction methods have also been used to predict the BBB permeability of triazole based compounds. For example, Arunrungvichian *et al.*[39] reported a series of substituted 1,2,3-triazoles as α7 nicotinic acetylcholine receptor agonists with predicted physiochemical properties such as pKa and logP to rationalize BBB permeability. Similarly, Ulloora *et al.* synthesized hybrids of imidazo[1,2-*a*] pyridines and 1,2,3-triazoles with antiepileptic *in vivo* effects with calculated clogP values in the range of 3.5–5.3, which confirmed their lipophilic nature and thus, a higher likelihood of entering the CNS.[40]

We used a web-based platform ADMETlab, designed based on the Django framework in Python for calculating chemical ADMET properties based on a comprehensively collected ADMET database.[41] The probability of drug candidates to cross the BBB depends upon parameters such as lipophilicity (cLogP), charges, flexibility, H-bond donors and acceptors, size (MW and number of rings) and shape, surface and volume descriptor and amphiphilicity.[42–47] Based on calculations, all Tr-series compounds (**Tr1**, **Tr3**, and **Tr5–Tr18**) showed satisfactory typical parameters that favour crossing of the BBB such as hydrogen bond donor <5, H-bond acceptors <10, rotatable bonds <10, molecular weight <750 Dalton, and cLogP <10 (ESI, Table S1†). In addition, calculated clogD values of our Tr

series compounds were in the range of 0.1–2.0 which confirmed a good balance between lipophilicity and solubility, a prerequisite for BBB penetration as discussed extensively by H. van de Waterbeemd *et al.*[48]

We also used BBB predictor "AlzPlatform" developed by Yuan *et al.*[42] to confirm whether a compound can cross the BBB or not. This predictor was built by applying the support vector machine (SVM) and LiCABEDS[49] algorithms on four types of fingerprints of 1593 reported compounds.[42] The calculated BBB permeability probability was found to be greater than 0.80 for all Tr series compounds except for **Tr7**, **Tr8** and **Tr9** (ESI Table S1†).

Conclusion

In conclusion, a set of triazole core-structure-based compounds was synthesized and evaluated as α-syn inhibitors. The designed molecules were synthesized using the azide–alkyne Huisgen cycloaddition approach. Later, the target molecules were evaluated for *in vitro* inhibition of α-syn fibrillogenesis and disaggregation. Compounds **Tr3**, **Tr7**, **Tr12**, **Tr15**, and **Tr16** inhibited the α-syn fibrillogenesis and further displayed the disaggregation activity when treated with the pre-aggregated α-syn. From *in silico* studies, we observed that these compounds exhibited good binding affinity with α-syn. All the compounds except **Tr11** did not exhibit any significant toxic effects on SH-SY5Y cell lines and can be further evaluated for their efficacy *in vivo*.

Experimental

Chemistry

Solvents, reagents, and other consumables used were purchased from different supplying companies and were used without further purification and activation. A Bruker 300 MHz FT spectrometer was used to obtain the NMR spectra of the synthesized target compounds. TMS (δ 0.00) was used as an internal standard to report proton chemical shifts in ppm. Solvents: $CDCl_3$ and DMSO were used to dissolve samples to record NMR ($CDCl_3$, δ 7.26; DMSO-d_6 δ 2.54). The multiplicities of NMR signals are designated as s (singlet), d (doublet), dd (double doublet), t (triplet), q (quartet), br (broad), and m (multiplet, for unresolved lines). LCMS of the compounds were obtained using an Ab Sciex 2000 Triple Quad. Column chromatography for the purification of the compounds was performed with alumina (60–120 mesh). Aluminium oxide coated TLC sheets were used for thin-layer chromatography. The developed plates were visualized under UV light. Anhydrous sodium sulfate was used to dry the organic extracts. Büchi rotavapor R-100 was used for evaporation of the solvents. An Elementar Vario analyser was used for the elemental analysis of the target compounds that were found to be within ±0.4% of the theoretical values.

General procedure for the synthesis of the target compounds (Tr1, Tr3, and Tr5–Tr18)

Differently substituted azide (20 mg, 0.23 mmol) and alkyne (0.28 mmol) were dissolved in a mixed solvent system ($THF:H_2O$, 1 : 2). A fresh aqueous solution of sodium ascorbate (0.12 mmol, 0.2 mL) was added to the reaction vessel, followed by the addition of a freshly prepared aqueous solution of $CuSO_4{\cdot}5H_2O$ (0.04 mmol, 0.2 mL). The yellow coloured reaction mixture was stirred at 80 °C for 16 hours. TLC confirmed the endpoint of the reaction. The reaction mixture was dried under vacuum without any work up and purified by column chromatography using ethylacetate: hexanes = 50 : 50. The desired products were obtained with a yield of 60–80%.

3-(4-(((7-Chloroquinolin-4-yl)oxy)methyl)-1*H*-1,2,3-triazol-1-yl)-1-(3,4-dimethoxyphenyl) propan-1-one (*Tr1*). Snow white cotton like solid, yield = 76% (R_f = 0.5 in 100% ethylacetate); m.p. 180–182 °C; ^{1}H NMR (300 MHz, $CDCl_3$) δ 8.75 (d, J = 5.5 Hz, 1H), 8.11 (d, J = 9.0 Hz, 1H), 8.02 (d, J = 2.1 Hz, 1H), 7.90 (s, 1H), 7.56 (dd, J = 8.4, 2.1 Hz, 1H), 7.48 (d, J = 2.1 Hz, 1H), 7.42 (dd, J = 9.0, 2.1 Hz, 1H), 6.94 (d, J = 5.1 Hz, 1H), 6.89 (d, J = 8.4 Hz, 1H), 5.41 (s, 2H), 4.86 (t, J = 6.0 Hz, 2H), 3.94 (d, J = 7.2 Hz, 6H), 3.66 (t, J = 6.0 Hz, 2H). ^{13}C NMR (75 MHz, $CDCl_3$) δ 194.99, 160.91, 153.99, 152.46, 149.70, 149.20, 142.28, 135.84, 129.07, 127.83, 126.63, 124.78, 123.51, 122.98, 119.74, 110.13, 109.83, 101.50, 62.24, 56.17, 56.02, 45.18, 38.10. LCMS: (ESI, m/z): $[M + H]^+$ calcd for $C_{23}H_{21}ClN_4O_4$ 453.1; found 453.0; anal. calcd for $C_{23}H_{21}ClN_4O_4$ C, 61.00; H, 4.67; Cl, 7.83; N, 12.37; O, 14.13%; found C, 61.29; H, 4.47; Cl, 7.99; N, 12.56; O, 14.31%.

1-((1-(3-(3,4-Dimethoxyphenyl)-3-oxopropyl)-1*H*-1,2,3-triazol-4-yl)methyl)-1*H*-indole-3-carbaldehyde (*Tr3*). Light brown solid, yield = 80% (R_f = 0.7 in 100% ethylacetate); m.p. 166–168 °C; ^{1}H NMR (300 MHz, $CDCl_3$) δ 9.98 (s, 1H), 8.30 (d, J = 9.3 Hz, 1H), 7.82 (s, 1H), 7.62 (s, 1H), 7.52 (d, J = 1.8 Hz, 1H), 7.50 (d, J = 1.8 Hz, 1H), 7.44 (s, 1H), 7.32 (dd, J = 3.9, 2.4 Hz, 1H), 7.27 (s, 1H), 6.86 (d, J = 8.4 Hz, 1H), 5.44 (s, 2H), 4.76 (t, J = 6.0 Hz, 2H), 3.94 (s, 3H), 3.91 (s, 3H), 3.58 (t, J = 6.3 Hz, 2H). ^{13}C NMR (75 MHz, $CDCl_3$) δ 194.96, 184.74, 153.95, 149.15, 142.16, 138.46, 137.00, 129.02, 125.39, 124.20, 123.87, 123.12, 122.97, 122.13, 118.53, 110.22, 110.16, 109.86, 56.14, 55.99, 45.22, 42.33, 37.94. LCMS: (ESI, m/z): $[M + H]^+$ calcd for $C_{23}H_{22}N_4O_4$ 419.1; found 419.1; anal. calcd for $C_{23}H_{22}N_4O_4$; C, 66.02; H, 5.30; N, 13.39; O, 15.29%; found C, 66.22; H, 5.50; N, 13.18; O, 15.56%.

1-(3,4-Dimethoxyphenyl)-3-(4-(hydroxymethyl)-1*H*-1,2,3-triazol-1-yl)propan-1-one (*Tr5*). Light brown solid, yield = 70% (R_f = 0.6 in 100% ethylacetate); m.p. 189–191 °C; ^{1}H NMR (300 MHz, $CDCl_3$) δ 7.72 (s, 1H), 7.55 (d, J = 10.5 Hz, 1H), 7.48 (s, 1H), 7.28 (s, 1H), 6.89 (d, J = 8.4 Hz, 1H), 4.80 (t, J = 6.3 Hz, 2H), 4.75 (s, 2H), 3.95 (s, 3H), 3.93 (s, 3H), 3.61 (t, J = 6.3 Hz, 2H). ^{13}C NMR (75 MHz, $CDCl_3$) δ 195.04, 153.86, 149.12, 147.42, 129.11, 123.22, 122.97, 110.10, 109.83, 56.15, 56.00, 45.00, 38.20, 29.70. LCMS: (ESI, m/z): $[M + H]^+$ calcd for $C_{14}H_{17}N_3O_4$ 292.1; found 292.1; anal. calcd for $C_{14}H_{17}N_3O_4$; C, 57.72; H,

5.88; N, 14.42; O, 21.97%; found C, 57.91; H, 5.99; N, 14.62; O, 21.77%.

(4-(((7-Chloroquinolin-4-yl)oxy)methyl)-1*H*-1,2,3-triazol-1-yl)(phenyl)-methanone (*Tr6*). Snow white solid, yield = 66% (R_f = 0.35 in 100% ethylacetate); m.p. 192–194 °C; ^{1}H NMR (300 MHz, $CDCl_3$) δ 7.86–7.78 (m, 5H), 7.53 (s, 1H), 7.51 (d, J = 0.12 Hz, 1H), 7.45 (d, J = 7.8 Hz, 4H), 7.42 (s, 1H), 6.25 (s, 1H), 1.85 (s, 2H). ^{1}H NMR (300 MHz, Chloroform-*d*) δ 7.89–7.73 (m, 5H), 7.53 (s, 1H), 7.51–7.43 (m, 5H), 6.25 (s, 2H). ^{13}C NMR (75 MHz, $CDCl_3$) δ 169.67, 133.42, 132.93, 131.98, 130.62, 128.62, 127.35, 123.31, 115.34, 113.39, 109.50, 107.58, 103.40, 97.61, 95.13, 85.75, 73.49. LCMS: (ESI, m/z): $[M + H]^+$ calcd for $C_{19}H_{13}ClN_4O_2$ 365.0; found 365.1; anal. calcd for $C_{19}H_{13}ClN_4O_2$; C, 62.56; H, 3.59; Cl, 9.72; N, 15.36; O, 8.77%; found C, 62.76; H, 3.80; Cl, 9.92; N, 15.56; O, 8.57%.

3-(4-(((2,7a-Dihydrobenzo[*d*]thiazol-2-yl)thio)methyl)-1*H*-1,2,3-triazol-1-yl)-1-(3,4-dimethoxyphenyl)propan-1-one (*Tr7*). Off white solid, yield = 61% (R_f = 0.75 in 100% ethylacetate); m.p. 200–202 °C; ^{1}H NMR (300 MHz, $CDCl_3$) δ 7.89 (d, J = 8.1 Hz, 1H), 7.77 (s, 1H), 7.74 (d, J = 7.8 Hz, 1H), 7.50 (dd, J = 8.4, 1.8 Hz, 2H), 7.42 (dd, J = 5.1, 2.1 Hz, 2H), 7.31 (d, J = 7.8 Hz, 1H), 7.26 (s, 1H), 6.85 (d, J = 8.4 Hz, 1H), 4.76 (t, J = 6.3 Hz, 2H), 4.67 (s, 2H), 3.94 (s, 3H), 3.90 (s, 3H), 3.58 (t, J = 6.6 Hz, 2H). ^{13}C NMR (75 MHz, $CDCl_3$) δ 194.97, 165.79, 153.89, 153.04, 149.17, 143.60, 135.46, 129.23, 126.06, 124.34, 124.21, 122.90, 121.55, 121.06, 110.13, 109.94, 56.12, 56.00, 45.15, 38.16, 27.77. LCMS: (ESI, m/z): $[M - H]^-$ calcd For $C_{21}H_{22}N_4O_3S_2$ 441.1; found 440.8; anal. calcd for $C_{21}H_{22}N_4O_3S_2$; C, 56.99; H, 5.01; N, 12.66; O, 10.85; S, 14.49%; found C, 56.76; H, 5.21; N, 12.88; O, 10.98; S, 14.69%.

1-(3,4-Dimethoxyphenyl)-3-(4-(((5-methoxy-3a,7a-dihydro-1*H*-benzo[*d*]imidazol-2-yl)thio)methyl)-1*H*-1,2,3-triazol-1-yl)propan-1-one (*Tr8*). Brown solid, yield = 66% (R_f = 0.45 in 100% ethylacetate); m.p. 199–201 °C; ^{1}H NMR (300 MHz, $CDCl_3$) δ 10.34 (s, 1H), 7.69 (s, 1H), 7.40 (s, 1H), 7.36 (d, J = 5.1 Hz, 1H), 7.32 (d, J = 9.0 Hz, 1H), 6.91 (d, J = 1.5 Hz, 1H), 6.76 (d, J = 8.4 Hz, 1H), 4.62 (t, J = 6.3 Hz, 2H), 4.33 (s, 1H), 3.82 (d, J = 8.4 Hz, 6H), 3.69 (s, 2H), 3.62 (s, 1H), 3.43 (t, J = 6.3 Hz, 2H), 2.21 (s, 1H), 2.00 (s, 3H). ^{13}C NMR (75 MHz, $CDCl_3$) δ 194.94, 176.73, 156.67, 153.92, 149.11, 147.62, 143.79, 129.00, 124.20, 123.01, 115.07, 112.70, 110.16, 109.95, 96.82, 56.05, 55.93, 55.70, 45.43, 37.82, 27.07, 20.91. LCMS: (ESI, m/z): $[M - H]^-$ calcd for $C_{22}H_{25}N_5O_4S$ 454.1; found 454.0; anal. calcd for $C_{22}H_{25}N_5O_4S$; C, 58.01; H, 5.53; N, 15.37; O, 14.05; S, 7.04%; found C, 58.21; H, 5.68; N, 15.57; O, 14.25; S, 7.34%.

7-((1-(3-(3,4-Dimethoxyphenyl)-3-oxopropyl)-1*H*-1,2,3-triazol-4-yl)methoxy)-4-methyl-2*H*-chromen-2-one (*Tr9*). Pale yellow solid, yield = 72% (R_f = 0.7 in 100% ethylacetate); m.p. 182–184 °C; ^{1}H NMR (300 MHz, $CDCl_3$) δ 7.85 (s, 1H), 7.56 (dd, J = 9.6, 1.8 Hz, 1H), 7.51 (s, 1H), 7.48 (s, 1H), 7.27 (s, 1H), 6.96 (d, J = 2.4 Hz, 1H), 6.91 (d, J = 4.8 Hz, 1H), 6.14 (s, 1H), 5.23 (s, 2H), 4.84 (t, J = 6.3 Hz, 2H), 3.95 (s, 3H), 3.93 (s, 3H), 3.64 (t, J = 6.0 Hz, 2H), 2.39 (s, 3H). ^{13}C NMR (75 MHz, $CDCl_3$) δ 194.94, 161.14, 155.01, 153.86, 152.57, 149.09, 142.59, 129.09, 125.67, 124.62, 122.94, 113.91, 112.48, 112.07, 110.18, 109.88, 101.95, 62.13, 56.11, 55.96, 45.15, 38.10, 29.65, 18.60. LCMS: (ESI, m/z): $[M + H]^+$ calcd for $C_{24}H_{23}N_3O_6$; 450.1; found 450.0; anal. calcd for $C_{24}H_{23}N_3O_6$; C, 64.14; H, 5.16; N, 9.35; O, 21.36%; found C, 64.34; H, 5.36; N, 9.55; O, 21.16%.

7-((1-(7-Chloroquinolin-4-yl)-1*H*-1,2,3-triazol-4-yl)methoxy)-4-methyl-2*H*-chromen-2-one (*Tr10*). Light chocolate coloured solid, yield = 68% (R_f = 0.4 in 100% ethylacetate); m.p. 190–192 °C; ^{1}H NMR (300 MHz, $CDCl_3$) δ 9.08 (d, J = 4.8 Hz, 1H), 8.26 (d, J = 1.8 Hz, 1H), 8.17 (s, 1H), 7.99 (d, J = 9.0 Hz, 1H), 7.62 (dd, J = 9.3, 2.1 Hz, 1H), 7.55–7.51 (m, 1H), 7.27 (s, 1H), 7.03 (d, J = 2.4 Hz, 1H), 7.00 (s, 1H), 6.17 (s, 1H), 5.44 (s, 2H), 2.42 (s, 3H). ^{13}C NMR (75 MHz, $CDCl_3$) δ 161.03, 160.91, 157.02, 155.19, 152.36, 151.37, 150.24, 144.03, 140.79, 137.09, 129.63, 129.08, 125.86, 124.76, 124.44, 120.18, 116.09, 112.52, 112.39, 102.14, 62.10, 18.67. LCMS: (ESI, m/z): $[M + H]^+$ calcd for $C_{22}H_{15}ClN_4O_3$ 419.0 found 418.9; anal. calcd for $C_{22}H_{15}ClN_4O_3$; C, 63.09; H, 3.61; Cl, 8.46; N, 13.38; O, 11.46%; found C, 63.29; H, 3.41; Cl, 8.26; N, 13.59; O, 11.68%.

1-((1-(7-Chloroquinolin-4-yl)-1*H*-1,2,3-triazol-4-yl)methyl)-1*H*-indole-3-carbaldehyde (*Tr11*). Light brown solid, yield = 69% (R_f = 0.35 in 100% ethylacetate); m.p. 188–190 °C; ^{1}H NMR (300 MHz, $CDCl_3$) δ 10.05 (s, 1H), 9.02 (d, J = 4.5 Hz, 1H), 8.34 (d, J = 6.9 Hz, 1H), 8.24 (s, 1H), 7.94 (s, 1H), 7.90–7.81 (m, 2H), 7.55 (dd, J = 16.2, 9.0 Hz, 2H), 7.38 (dd, J = 12.9, 5.1 Hz, 2H), 7.26 (s, 1H), 5.67 (s, 2H). ^{13}C NMR (75 MHz, $CDCl_3$) δ 184.59, 153.64, 151.27, 150.19, 146.46, 143.72, 139.89, 137.89, 136.93, 134.91, 129.66, 129.08, 124.52, 124.24, 123.85, 123.38, 122.47, 119.08, 116.00, 109.94, 42.49. LCMS: (ESI, m/z): $[M + H]^+$ calcd for $C_{21}H_{14}ClN_5O$ 388.0; found 387.9; anal. calcd for $C_{21}H_{14}ClN_5O$; C, 65.04; H, 3.64; Cl, 9.14; N, 18.06; O, 4.13%; found C, 65.25; H, 3.87; Cl, 9.35; N, 18.00; O, 4.02%.

2-(((1-(7-Chloroquinolin-4-yl)-1*H*-1,2,3-triazol-4-yl)methyl)thio)benzo[*d*]thiazole (*Tr12*). White solid, yield = 70% (R_f = 0.4 in 100% ethylacetate); m.p. 155–157 °C; ^{1}H NMR (300 MHz, $CDCl_3$) δ 9.02 (s, 1H), 8.18 (d, J = 20.1 Hz, 2H), 7.91–7.84 (m, 1H), 7.84–7.74 (m, 2H), 7.45 (d, J = 7.5 Hz, 2H), 7.38–7.19 (m, 2H), 4.83 (s, 2H). ^{13}C NMR (75 MHz, $CDCl_3$) δ 152.93, 151.38, 150.17, 145.10, 140.83, 137.60, 136.86, 135.58, 129.42, 129.02, 126.23, 125.03, 124.64, 124.35, 121.48, 121.26, 120.49, 116.05, 27.42. LCMS: (ESI, m/z): $[M + 2]^+$ calcd for $C_{19}H_{12}ClN_5S_2$ 411.0; found 411.8; anal. calcd for $C_{19}H_{12}ClN_5S_2$; C, 55.67; H, 2.95; Cl, 8.65; N, 17.09; S, 15.64%; found C, 55.88; H, 2.74; Cl, 8.85; N, 17.28; S, 15.81%.

7-Chloro-4-(4-(((5-methoxy-1*H*-benzo[*d*]imidazol-2-yl)thio)methyl)-1*H*-1,2,3-triazol-1-yl)quinoline (*Tr13*). Yellow solid, yield = 61% (R_f = 0.6 in 100% ethylacetate); m.p. 210–212 °C; ^{1}H NMR (300 MHz, chloroform-*d*) δ 8.96 (s, 1H), 8.11 (s, 3H), 7.69 (d, J = 9.3 Hz, 1H), 7.45–7.31 (m, 3H), 6.92 (s, 1H), 6.75 (d, J = 8.7 Hz, 1H), 4.63 (s, 2H), 3.76 (s, 3H). ^{13}C NMR (75 MHz, $CDCl_3$) δ 184.66, 179.29, 155.88, 151.34, 149.86, 145.28, 140.59, 138.08, 136.36, 129.07, 128.63, 124.96, 124.34, 121.73, 120.26, 116.02, 111.39, 111.00, 55.64, 26.67. LCMS: (ESI, m/z): $[M + H]^+$ calcd for $C_{20}H_{15}ClN_6OS$ 423.0; found 422.9; anal. calcd for $C_{20}H_{15}ClN_6OS$; C, 56.80; H, 3.58; Cl, 8.38; N, 19.87; O, 3.78; S, 7.58%; found C, 56.98; H, 3.79; Cl, 8.58; N, 19.57; O, 3.58; S, 7.77%.

3-(4-((3-Acetylphenoxy)methyl)-1*H*-1,2,3-triazol-1-yl)-1-(3,4-dimethoxy-phenyl)propan-1-one (*Tr14*). Straw coloured solid, yield = 74% (R_f = 0.75 in 100% ethylacetate); m.p. 198–200 °C; ^{1}H NMR (300 MHz, $CDCl_3$) δ 7.83 (s, 1H), 7.57 (s, Hz, 2H), 7.54 (d, J = 1.8 Hz, 1H), 7.48 (d, J = 1.8 Hz, 1H), 7.37 (t, J = 8.1 Hz, 1H), 7.19 (dd, J = 8.4, 2.4 Hz, 1H), 6.89 (d, J = 8.4 Hz, 1H), 5.22 (s, 2H), 4.83 (t, J = 6.3 Hz, 2H), 3.95 (s, 3H), 3.93 (s, 3H), 3.64 (t, J = 6.0 Hz, 2H), 2.59 (s, 3H). ^{13}C NMR (75 MHz, $CDCl_3$) δ 197.86, 194.99, 158.35, 153.79, 149.02, 143.16, 138.37, 129.66, 129.06, 124.45, 122.92, 121.40, 119.90, 113.74, 110.15, 109.86, 61.80, 56.04, 55.89, 45.12, 38.05, 26.64. LCMS: (ESI, m/z): $[M + H]^+$ calcd for $C_{22}H_{23}N_3O_5$ 410.1; found 410.1; anal. calcd for $C_{22}H_{23}N_3O_5$; C, 64.54; H, 5.66; N, 10.26; O, 19.54%; found C, 64.74; H, 5.86; N, 10.29; O, 19.75%.

1-((1-(3-(3,4-Dimethoxyphenyl)-3-oxopropyl)-1*H*-1,2,3-triazol-4-yl)methyl) indoline-2,3-dione (*Tr15*). Fast yellow solid, yield = 67% (R_f = 0.4 in 100% ethylacetate); m.p. 206–208 °C; ^{1}H NMR (300 MHz, $CDCl_3$) δ 7.76 (s, 1H), 7.52–7.47 (m, 4H), 7.26 (s, 1H), 7.11 (d, J = 7.8 Hz, 1H), 6.86 (d, J = 8.7 Hz, 1H), 5.00 (s, 2H), 4.78 (s, 2H), 3.94 (s, 6H), 3.58 (s, 2H). ^{1}H NMR (300 MHz, chloroform-*d*) δ 7.76 (s, 1H), 7.62–7.44 (m, 3H), 7.26 (s, 2H), 7.10 (dd, J = 7.8, 4.5 Hz, 1H), 6.86 (d, J = 8.7 Hz, 1H), 5.00 (s, 2H), 4.78 (s, 2H), 3.94 (s, 6H), 3.59 (s, 2H). ^{13}C NMR (75 MHz, $CDCl_3$) δ 194.72, 178.49, 172.13, 153.96, 150.30, 149.22, 141.52, 138.52, 129.13, 125.27, 124.17, 123.94, 122.91, 117.54, 111.49, 110.14, 109.98, 56.13, 56.01, 45.26, 37.99, 35.38. LCMS: (ESI, m/z): $[M + H]^+$ calcd for $C_{22}H_{20}N_4O_5$ 421.1; found 420.9; anal. calcd for $C_{22}H_{20}N_4O_5$; C, 62.85; H, 4.80; N, 13.33; O, 19.03%; found C, 62.99; H, 4.62; N, 13.57; O, 19.20%.

3-(4-((2-Acetylphenoxy)methyl)-1*H*-1,2,3-triazol-1-yl)-1-(3,4-dimethoxy-phenyl)propan-1-one (*Tr16*). Faded yellow solid, yield = 78% (R_f = 0.5 in 100% ethylacetate); m.p. 187–189 °C; ^{1}H NMR (300 MHz, $CDCl_3$) δ 7.84 (s, 1H), 7.70 (dd, J = 7.8, 1.8 Hz, 1H), 7.55 (dd, J = 8.4, 2.1 Hz, 1H), 7.51–7.38 (m, 2H), 7.11 (d, J = 8.4 Hz, 1H), 7.01 (t, J = 7.5 Hz, 1H), 6.88 (d, J = 8.4 Hz, 1H), 5.27 (s, 2H), 4.83 (t, J = 6.0 Hz, 2H), 3.94 (s, 3H), 3.92 (s, 3H), 3.63 (t, J = 6.3 Hz, 2H), 2.55 (s, 3H). ^{13}C NMR (75 MHz, $CDCl_3$) δ 199.80, 194.96, 157.42, 153.94, 149.17, 143.08, 133.62, 130.37, 129.13, 128.78, 124.40, 122.94, 121.18, 113.00, 110.18, 109.92, 62.39, 56.12, 55.99, 45.17, 38.09, 31.88. LCMS: (ESI, m/z): $[M + H]^+$ calcd for $C_{22}H_{23}N_3O_5$ 410.1; found 410.1; anal. calcd for $C_{22}H_{23}N_3O_5$; C, 64.54; H, 5.66; N, 10.26; O, 19.54%; found C, 64.75; H, 5.87; N, 10.06; O, 19.05%.

1-(2-((1-(7-Chloroquinolin-4-yl)-1*H*-1,2,3-triazol-4-yl)methoxy) phenyl)ethan-1-one (*Tr17*). White solid, yield = 75% (R_f = 0.3 in 100% ethylacetate); m.p. 201–203 °C; ^{1}H NMR (300 MHz, $CDCl_3$) δ 7.83 (s, 2H), 7.62 (s, 2H), 7.57 (d, J = 7.8 Hz, 2H), 7.38 (t, J = 7.2 Hz, 2H), 7.20 (d, J = 8.1 Hz, 2H), 5.30 (s, 2H), 2.60 (s, 3H). ^{13}C NMR (75 MHz, $CDCl_3$) δ 197.70, 158.31, 151.38, 150.22, 144.65, 140.84, 138.67, 137.01, 129.90, 129.57, 129.05, 124.64, 124.49, 121.95, 120.57, 120.14, 116.08, 113.51, 61.93, 26.74. LCMS: (ESI, m/z): $[M + K]^+$ calcd for $C_{20}H_{15}ClN_4O_2$ 417.0; found 415.0; anal. calcd for $C_{20}H_{15}ClN_4O_2$; C, 63.41; H, 3.99; Cl, 9.36; N, 14.79; O, 8.45%; found; C, 63.55; H, 3.79; Cl, 9.56; N, 14.89; O, 8.26%.

1-(3-((1-(7-Chloroquinolin-4-yl)-1*H*-1,2,3-triazol-4-yl)methoxy) phenyl) ethan-1-one (*Tr18*). Cream white solid, yield = 66% (R_f = 0.25 in 100% ethylacetate); m.p. 188–190 °C; ^{1}H NMR (300 MHz, $CDCl_3$) δ 9.07 (d, J = 4.5 Hz, 1H), 8.25 (s, 1H), 8.15 (s, 1H), 7.98 (d, J = 9.0 Hz, 1H), 7.69–7.56 (m, 3H), 7.53 (s, 1H), 7.43 (t, J = 7.8 Hz, 1H), 7.28 (s, 1H), 5.42 (s, 2H), 2.62 (s, 3H). ^{13}C NMR (75 MHz, $CDCl_3$) δ 197.70, 158.31, 151.38, 150.22, 144.65, 140.84, 138.67, 137.01, 129.90, 129.57, 129.05, 124.64, 124.49, 121.95, 120.57, 120.14, 116.08, 113.51, 61.93, 26.74. LCMS: (ESI, m/z): $[M + H]^+$ calcd for $C_{20}H_{15}ClN_4O_2$ 379.0; found 379.1; anal. calcd for $C_{20}H_{15}ClN_4O_2$; C, 63.41; H, 3.99; Cl, 9.36; N, 14.79; O, 8.45%; found C, 63.62; H, 4.09; Cl, 9.56; N, 14.87; O, 8.36%.

Biological evaluation of the Tr-series compounds

α-Syn protein expression and purification. Recombinant human α-synuclein protein was expressed and purified by the osmotic shock method according to our previously reported protocol with slight modification in the elution strategy. Gradient elution was performed using different concentrations of NaCl such as 100 mM, 200 mM, 300 mM, and 500 mM with 20 mM Na phosphate (pH 8.0) to obtain protein fractions containing only α-syn. The characterisation of purified α-syn was performed by 15% SDS-PAGE and by western blot using a H3C antibody (Development Studies Hybridoma Bank). Dialysis was performed against water at 4 °C for the obtained α-syn protein for 7 h and it was allowed to lyophilise. After lyophilisation, protein was stored at −80 °C to determine aggregation kinetics.[25]

Preformed aggregate free α-syn preparation. Reconstitution of α-syn was performed in PB buffer (20 mM Na phosphate) (pH 7.4). After reconstitution, 1 M NaOH was used to adjust the pH of the solution around 11.0 for dissolution of preformed aggregates. The pH was again adjusted to 7.4 slowly by adding diluted HCl after 15 min. Furthermore, ultra-centrifugation was performed at 100 000*g* at 4 °C for 1 h for the removal of previously formed aggregates using a Beckman Ultra Centrifuge. The collected supernatant was allowed to filter through a 0.22 μM filter for the removal of particulate matter. The α-syn protein concentration was measured using an extinction coefficient of 5120 M^{-1} cm^{-1} by absorbance at 280 nm using Nanodrop.[50]

Monitoring aggregation kinetics of α-syn in the presence of Tr series compounds. Tr series compound stock solutions were prepared in DMSO because of their insoluble nature. The stock solution of ThT (5 mM) was made in PB buffer (20 mM Na Phosphate), pH 7.4, and filtered using a 0.22 μm filter for the removal of particulate matter. The α-syn aggregation was performed in the buffer (20 mM Na phosphate) (pH 7.4) at 37 °C using a 70 μM concentration. The prepared monomeric α-syn mixed with ThT (20 μM) and 0.01% Na azide in PB buffer was transferred into a 384 well flat bottom black plate (BRAND). Glass-beads (Sigma) (3–4 mm) were placed in the individual wells to achieve consistency in the aggregation kinetics. The sealing of the plate was done using a Nunc transparent film. As a positive control, we used α-syn with 10% DMSO.

For monitoring the inhibitory capabilities of the compounds to α-syn aggregation, a 1 : 1 M ratio of the compounds (**Tr series**) to α-syn was used. We used a total volume of 45 μL of the sample and it was transferred into each well. We used 4 wells for the control (α-syn) and each inhibitor (Tr-series compounds). The incubation of the plate was performed in the plate reader (Tecan Infinite M200 pro multimode) at 37 °C. The kinetics of α-syn fibrillation was analysed by measuring time-dependent changes in the fluorescence emission intensity of ThT at 485 nm (Ex: 440 nm) till the plateau phase obtained for the control and compounds (Tr series) at 30 min intervals with orbital shaking (30 s) prior to every time point. The graphs were produced using Origin 2017 software. Here, the average ± standard error of the mean (SEM) of n = 4 was considered for data representation.

Further analysis of the ThT fluorescence values was performed by fitting a curve into a sigmoidal curve through an equation where fluorescence intensity (Y) was a function of time t, the intercepts of the initial baseline and plateau intensity were represented by y_i and y_f with the y-axis, slopes were represented by m_i and m_f and fixed to zero in analysis, and the time required to obtain half the plateau phase fluorescence intensity was represented by $t_{1/2}$. The calculation of elongation time constant (τ) was performed by fitting the data in the below equation for individual 4 wells and then averaging was done to reduce biasness as mentioned earlier.[29]

$$Y = y_i + m_i t + \frac{y_f + m_f t}{1 + e^{-[(t-t_{1/2})/\tau]}}$$

The apparent rate constant (k_{app}) was calculated using the equation which is $1/\tau$ which represents the growth of synuclein fibrils. The time needed for nucleus formation (t_{lag}) was determined from the intercept between the lag and the elongation phase extrapolations. Student's t-test was carried out for the statistical difference with the probability (p) value less than 0.05 using GraphPad Prism 8.0 version software.

Fluorescence microscopy. After reaching the plateau phase in ThT aggregation kinetics, the sample was taken for fluorescence microscopy to see if there are any visible aggregates or not in α-syn alone and also in α-syn in the presence of compounds. A volume of 8 μL of α-syn alone and α-syn treated with the **Tr** series compounds in the presence of ThT dye was taken and added to a microscopic slide. After adding on the microscopic slide, it was covered with a coverslip. Furthermore, the extra solution was drained to prevent the floating of the solution. Fluorescence imaging was performed using a Zeiss Axio Observer inverted fluorescence microscope through a fluorescein isothiocyanate filter (FITC) and with 100× resolution. For imaging, the laser power and fluorescence intensity of the α-syn control and α-syn incubated with the Tr-series compounds were maintained constant throughout the analysis.

Fibril disassembly assay for Tr-series compounds. To identify the disaggregation property of the Tr-series compound on preformed fibrous species, α-syn protein at a 70 μM concentration was allowed to incubate as previously done in a 384 well flat bottom black plate (BRAND) at 37 °C until it reaches the plateau phase. After reaching the plateau phase, the Tr-series compounds were added in the same molar ratio (70 μM) as α-syn control and further incubated for 4–5 days in the absence of ThT to observe their disaggregation property. Here, only the α-syn control was incubated in the absence of ThT. We performed disaggregation assay in 1 well for the control and each compound. Furthermore, these samples were collected after incubation and their fibril disassembly was confirmed by fluorescence microscopy.

Fluorescence microscopy imaging of fibril disassembly assay in the presence of the Tr-series compounds. Fluorescence microscopy was performed to examine the disaggregation ability of the Tr-series compounds. Here 20 μM ThT dye was added to pre-formed aggregates of the α-syn sample and also pre-formed aggregates of α-syn with the Tr-series compounds since fibril disassembly assay was performed in the absence of ThT. After adding ThT, 8 μl volume of sample was taken and transferred to a clean microscopic slide. The microscopic slide was further covered with a coverslip and the excess solution has been drained. Furthermore, fluorescence imaging was performed using the Zeiss Axio Observer inverted fluorescence microscope with the FITC filter and 100× resolution. The laser power and fluorescence intensity of α-syn (control) and α-syn incubated with the Tr-series compounds were maintained constant throughout the analysis.

Docking protocol. The Pdb file of α-syn (PDB ID 1XQ8) was obtained from the Protein Data Bank (http://www.rcsb.org).[51] AutoDock Vina version 1.5.6 was used to perform docking and redocking of the protein with the ligand molecules. Molecular interactions between the key residues of the protein and the ligands were visualized using PyMOL, a visualization tool. Different non-covalent interactions such as π–π stacking interactions and H-bonding were detected, while the ligand molecules were found lying within a range of 2.5 Å. In addition, the binding free energy of the ligands was calculated and the result supports the *in vitro* results and provides a plausible mechanism of action of these compounds for inhibiting α-syn fibrillogenesis.

Cytotoxicity assay. SH-SY5Y cells were cultured in DMEM/F12 supplemented with 10% heat-inactivated FBS and 1% penicillin/streptomycin. On 80% of the cell growth, confluent cells were trypsinized and 2–3 × 10^5 cells were transferred into a transparent 96 well plate. Furthermore, the cells were allowed to incubate for 24 h at 37 °C in a humid environment of 5% CO_2. After incubation, the media were removed and the test compounds were transferred in triplicate and incubated again for 24 h. The media were replaced with fresh media with MTT reagent (3-(4,5-dimethylthiazol-2-yl)-2,5-diphenyltetrazoliumbromide) (0.5 mg ml^{-1}) and transferred into a transparent 96 well plate having cells and incubated again for 4 h at 37 °C, with 5% CO_2 in the dark. After completion of the incubation period, the media were removed, and formazan crystals were allowed to dissolve in 100 μl DMSO. The plate was kept at 37 °C for 30 min followed by absorbance measurement at 570 nm in a microplate reader (BioTek SYNERGYH1, 3.04.17).

Here, the average ± standard error of the mean (SEM) of $n = 4$ was considered for data representation.

Author contributions

MM and AS designed and synthesized the compounds. JG and SG planned experiments for various biophysical assays. JG performed all biophysical assays. PH performed cytotoxicity assays. MM, NH, JG and SG wrote the manuscript.

Conflicts of interest

There are no conflicts to declare.

Acknowledgements

MM thanks the CSIR, Govt. of India for financial assistance in the form of a senior research fellowship (SRF). JG thanks DBT-JRF for the Ph.D. fellowship. AS is grateful to the UGC for the Rajiv Gandhi national fellowship. PH thanks the MHRD for the Ph.D. fellowship and additional fellowship during the Ph.D. Programme from IIT Gandhinagar. SG acknowledges the SERB, Govt. of India (CRG/2018/004960) for partial funding support.

References

1 E. Borrell, *J. Neurosci. Nurs.*, 2000, **32**, 254–255.
2 A. Elbaz, L. Carcaillon, S. Kab and F. Moisan, *Rev. Neurol.*, 2016, **172**, 14–26.
3 E. R. Dorsey, A. Elbaz, E. Nichols, F. Abd-Allah, *et al.*, *Lancet Neurol.*, 2018, **17**, 939–953.
4 D. D. Truong and R. Bhidayasiri, *In International Neurology*, Wiley-Blackwell, 2nd edn, 2016.
5 B. Mollenhauer, J. J. Locascio, W. Schulz-Schaeffer, F. Sixel-Döring, C. Trenkwalder and M. G. Schlossmacher, *Lancet Neurol.*, 2011, **10**, 230–240.
6 S. Slaets, E. Vanmechelen, N. Le Bastard, H. Decraemer, M. Vandijck, J.-J. Martin, P. P. De Deyn and S. Engelborghs, *Alzheimer's Dementia*, 2014, **10**, S290–S298.
7 C. Harnois and T. Di Paolo, *Invest. Ophthalmol. Visual Sci.*, 1990, **31**, 2473–2475.
8 H. Braak and K. Del Tredici, *Adv. Anat., Embryol. Cell Biol.*, 2009, **201**, 1–119.
9 M. Zhu, Z.-J. Qin, D. Hu, L. A. Munishkina and A. L. Fink, *Biochemistry*, 2006, **45**, 8135–8142.
10 T. R. Alderson and J. L. Markley, *Intrinsically Disord. Proteins*, 2013, **1**, e26255.
11 S. Peña-Díaz, J. Pujols, M. Conde-Giménez, A. Čarija, E. Dalfo, J. García, S. Navarro, F. Pinheiro, J. Santos, X. Salvatella, J. Sancho and S. Ventura, *Front. Mol. Neurosci.*, 2019, **12**, 1–12.
12 J. Pujols, S. Peña-Díaz, D. F. Lázaro, F. Peccati, F. Pinheiro, D. González, A. Carija, S. Navarro, M. Conde-Giménez, J. García, S. Guardiola, E. Giralt, X. Salvatella, J. Sancho, M. Sodupe, T. F. Outeiro, E. Dalfó and S. Ventura, *Proc. Natl. Acad. Sci. U. S. A.*, 2018, **115**, 10481–10486.
13 D. Yedlapudi, G. S. Joshi, D. Luo, S. V. Todi and A. K. Dutta, *Sci. Rep.*, 2016, **6**, 38510.
14 B. H. Dahl, G. M. Olsen, J. K. Christensen and D. Peters, CA2735773A12010/03/11, 2011.
15 A. K. Jain, C. Karthikeyan, K. D. McIntosh, A. K. Tiwari, P. Trivedi and A. DuttKonar, *New J. Chem.*, 2019, **43**, 1202–1215.
16 J. Carlsson, D. K. Tosh, K. Phan, Z.-G. Gao and K. A. Jacobson, *ACS Med. Chem. Lett.*, 2012, **3**, 715–720.
17 P. Van der Veken, V. Fülöp, D. Rea, M. Gerard, R. Van Elzen, J. Joossens, J. D. Cheng, V. Baekelandt, I. De Meester, A.-M. Lambeir and K. Augustyns, *J. Med. Chem.*, 2012, **55**, 9856–9867.
18 C. Fischer, A. J. Schell and B. Munoz, *Merck Sharp & Dohme Corp., Rahway, NJ (US)*, US8575150B2, 2013.
19 P. H. Olesen, A. R. Sørensen, B. Ursø, P. Kurtzhals, A. N. Bowler, U. Ehrbar and B. F. Hansen, *J. Med. Chem.*, 2003, **46**, 3333–3341.
20 E. A. Luke, M. C. Yadon, J. Cummings, M. Hudson, T. Lake and Q. Hu, *et al.*, *ProteoTech Inc., Kirkland, WA (US)*, US2013/0338202A1, 2013.
21 B. M. Vincent, D. F. Tardiff, J. S. Piotrowski, R. Aron, M. C. Lucas, C. Y. Chung, H. Bacherman, Y. Chen, M. Pires, R. Subramaniam, D. B. Doshi, H. Sadlish, W. K. Raja, E. J. Solís, V. Khurana, B. Le Bourdonnec, R. H. Scannevin and K. J. Rhodes, *Cell Rep.*, 2018, **25**, 2742–2754.
22 A. P. Kozikowski, I. N. Gaisina, P. A. Petukhov, J. Sridhar, L. T. King, S. Y. Blond, T. Duka, M. Rusnak and A. Sidhu, *ChemMedChem*, 2006, **1**, 256–266.
23 W. Chu, D. Zhou, V. Gaba, J. Liu, S. Li, X. Peng, J. Xu, D. Dhavale, D. P. Bagchi, A. D'Avignon, N. B. Shakerdge, B. J. Bacskai, Z. Tu, P. T. Kotzbauer and R. H. Mach, *J. Med. Chem.*, 2015, **58**, 6002–6017.
24 S. Kumar, A. Saini, J. Gut, P. J. Rosenthal, R. Raj and V. Kumar, *Eur. J. Med. Chem.*, 2017, **138**, 993–1001.
25 C. Huang, G. Ren, H. Zhou and C. Wang, *Protein Expression Purif.*, 2005, **42**, 173–177.
26 M. Maqbool, J. Gadhavi, P. Hivare, S. Gupta and N. Hoda, *Eur. J. Med. Chem.*, 2020, 112705.
27 H. Naiki, K. Higuchi, M. Hosokawa and T. Takeda, *Anal. Biochem.*, 1989, **177**, 244–249.
28 L. P. Jameson, N. W. Smith and S. V. Dzyuba, *ACS Chem. Neurosci.*, 2012, **3**, 807–819.
29 K. Gade Malmos, L. M. Blancas-Mejia, B. Weber, J. Buchner, M. Ramirez-Alvarado, H. Naiki and D. Otzen, *Amyloid*, 2017, **24**, 1–16.
30 O. Trott and A. J. Olson, *J. Comput. Chem.*, 2010, **31**, 455–461.
31 K. Uéda, H. Fukushima, E. Masliah, Y. Xia, A. Iwai, M. Yoshimoto, D. A. Otero, J. Kondo, Y. Ihara and

T. Saitoh, *Proc. Natl. Acad. Sci. U. S. A.*, 1993, **90**, 11282–11286.
32 B. I. Giasson, I. V. J. Murray, J. Q. Trojanowski and V. M.-Y. Lee, *J. Biol. Chem.*, 2001, **276**, 2380–2386.
33 M. D. Tuttle, G. Comellas, A. J. Nieuwkoop, D. J. Covell, D. A. Berthold, K. D. Kloepper, J. M. Courtney, J. K. Kim, A. M. Barclay, A. Kendall, W. Wan, G. Stubbs, C. D. Schwieters, V. M. Y. Lee, J. M. George and C. M. Rienstra, *Nat. Struct. Mol. Biol.*, 2016, **23**, 409–415.
34 W. M. Pardridge, *NeuroRX*, 2005, **2**, 3–14.
35 P. B. Wingrove, K. A. Wafford, C. Bain and P. J. Whiting, *Proc. Natl. Acad. Sci. U. S. A.*, 1994, **91**, 4569–4573.
36 J. C. Verster and E. R. Volkerts, *CNS Drug Rev.*, 2006, **10**, 45–76.
37 B. Kaproń, J. J. Łuszczki, A. Siwek, T. Karcz, G. Nowak, M. Zagaja, M. Andres-Mach, A. Stasiłowicz, J. Cielecka-Piontek, J. Kocki and T. Plech, *Bioorg. Chem.*, 2020, **94**, 103355–103365.
38 S.-E. Tsai, S.-M. Li, C.-C. Tseng, C.-Y. Chung, Y.-H. Zeng, C. Chieh Lin, M.-T. Fuh, L.-C. Yang, Y.-C. Yang and F.-F. Wong, *Bioorg. Chem.*, 2020, **104**, 104299.
39 K. Arunrungvichian, V. V. Fokin, O. Vajragupta and P. Taylor, *ACS Chem. Neurosci.*, 2015, **6**, 1317–1330.
40 S. Ulloora, R. Shabaraya and A. V. Adhikari, *Bioorg. Med. Chem. Lett.*, 2013, **23**, 3368–3372.
41 J. Dong, N.-N. Wang, Z.-J. Yao, L. Zhang, Y. Cheng, D. Ouyang, A.-P. Lu and D.-S. Cao, *J. Cheminf.*, 2018, **10**, 29.
42 Y. H. Zhao, M. H. Abraham, A. Ibrahim, P. V. Fish, S. Cole, M. L. Lewis, M. J. de Groot and D. P. Reynolds, *J. Chem. Inf. Model.*, 2007, **47**, 170–175.
43 K. M. M. Doan, J. E. Humphreys, L. O. Webster, S. A. Wring, L. J. Shampine, C. J. Serabjit-Singh, K. K. Adkison and J. W. Polli, *J. Pharmacol. Exp. Ther.*, 2002, **303**, 1029–1037.
44 T. J. Hou, W. Zhang, K. Xia, X. B. Qiao and X. J. Xu, *J. Chem. Inf. Comput. Sci.*, 2004, **44**, 1585–1600.
45 J. Kai, K. Nakamura, T. Masuda, I. Ueda and H. Fujiwara, *J. Med. Chem.*, 1996, **39**, 2621–2624.
46 H. Li, C. W. Yap, C. Y. Ung, Y. Xue, Z. W. Cao and Y. Z. Chen, *J. Chem. Inf. Model.*, 2005, **45**, 1376–1384.
47 J. Duan, S. L. Dixon, J. F. Lowrie and W. Sherman, *J. Mol. Graphics Modell.*, 2010, **29**, 157–170.
48 H. van de Waterbeemd, G. Camenisch, G. Folkers, J. R. Chretien and O. A. Raevsky, *J. Drug Targeting*, 1998, **6**, 151–165.
49 X.-Q. Xie, J.-Z. Chen and E. M. Billings, *Proteins: Struct., Funct., Genet.*, 2003, **53**, 307–319.
50 X. Meng, L. A. Munishkina, A. L. Fink and V. N. Uversky, *Parkinson's Dis.*, 2010, **2010**, 1–16.
51 V. M. S. Gil and N. C. Oliveira, *J. Chem. Educ.*, 1990, **67**, 473.